LA-UR- 08-7243

Approved for public release;
distribution is unlimited.

Title:	Universal size dependence of Auger constants in direct- and indirect-gap semiconductor nanocrystals
Author(s):	Istvan Robel, Ryan Gresback, Uwe Kortshagen, Richard D. Schaller, and Victor I. Klimov
Intended for:	Publication in the scientific journal Nature Physics

Form 836 (7/06)

Universal size dependence of Auger constants in direct- and indirect-gap semiconductor nanocrystals

István Robel[1], Ryan Gresback[2], Uwe Kortshagen[2], Richard D. Schaller[1]*, and Victor I. Klimov[1]*

[1]*Chemistry Division, Los Alamos National Laboratory, Los Alamos, New Mexico 87545, USA*

[2]*Department of Mechanical Engineering, University of Minnesota, Minneapolis, Minnesota 55455, USA*

Three-dimensional (3D) spatial confinement of electronic wave functions in semiconductor nanocrystals (NCs) results in a significant enhancement of multi-electron phenomena including nonradiative Auger recombination[1-4]. In this process, a conduction-band electron recombines with a valence-band hole by transferring the recombination energy to a third carrier. Significant interest in Auger recombination in NCs has been stimulated by recent studies of NC lasing[5,6] and generation-III photovoltaics enabled by carrier multiplication[7-9] because in both of these prospective applications Auger recombination represents a dominant carrier-loss mechanism. Here, we perform a side-by-side comparison of Auger recombination rates in NCs of several different compositions including Ge, PbSe, InAs, and CdSe. We observe that the only factor, which has a significant effect on the measured recombination rates, is the size of the NCs but not the details of the material's electronic structure. Most surprisingly, comparable rates are measured for nanocrystals of direct- and indirect-gap semiconductor NCs despite a dramatic four-to-five orders of magnitude difference in respective bulk-semiconductor Auger constants. This unusual observation can

be explained by confinement-induced relaxation of momentum conservation, which smears out the difference between direct- and indirect-gap materials.

In direct-gap bulk semiconductors, the conduction- and valence-band minima are co-located in momentum (***k***) space. In this case, Auger recombination occurs as a three-particle process wherein the electron-hole recombination energy is transferred via the Coulomb interaction to the third carrier (an electron or a hole) re-exciting it to a higher-energy state[10] (Fig. 1a). Because of combined requirements of energy and translational momentum conservation, this process exhibits a thermally activated behavior[10,11] and is characterized by a rate (r_A) that scales as $r_A \propto \exp(-E_A/k_BT)]$, where k_B is the Boltzmann constant, T is the temperature, and E_A is the activation threshold, which is directly proportional to the energy gap, E_g. The corresponding rate equation is $dn/dt = -C_An^3$, where n is the carrier density and C_A is the Auger constant.

In indirect-gap bulk materials, carriers involved in Auger recombination are separated in ***k***-space (Fig. 1b); therefore, Auger decay occurs with appreciable efficiencies only with participation of momentum-conserving phonons[11] (dashed arrow in Fig. 1b). While involvement of phonons removes the activation barrier, it leads to a significant reduction of the decay rate because such Auger recombination is a higher-order, four-particle process[11] (Fig. 1b). For example, direct-gap InAs and indirect-gap Ge, exhibit room-temperature Auger constants that differ by five orders of magnitude ($1.1\text{x}10^{-26}$ cm^6s^{-1} vs. $1.1\text{x}10^{-31}$ cm^6s^{-1}, respectively[12,13]), despite a relatively small difference in energy gaps (0.35 eV and 0.66 eV, respectively).

Strong 3D spatial confinement, characteristic of ultrasmall semiconductor NCs, leads to relaxation of translational momentum conservation, which should diminish the distinction between direct- and indirect-gap semiconductors with regard to the Auger process (Fig. 1c).

Whereas the effect of 3D confinement on radiative recombination in indirect-gap materials has been extensively analyzed in the literature[14,15], the influence of quantum confinement on multiparticle processes such as Auger recombination in indirect-gap semiconductors has not been systematically studied either theoretically or experimentally.

The purpose of this work is to address this unexplored aspect of Auger recombination by performing a comparative study of Auger-decay rates in NCs of direct- and indirect-gap semiconductors. Specifically, we study multi-electron-hole-pair (multiexciton) recombination dynamics in NCs of indirect-gap Ge, and compare them with results for NCs of direct-gap InAs, PbSe, and CdSe[2]. We observe that the effective Auger constant for all of these materials can be described by the universal cubic size dependence $C_A \propto R^3$. Even more remarkable is that the absolute values of Auger constants in NCs of the same size but different compositions are similar despite a dramatic orders-of-magnitude difference in C_A values in the respective bulk solids. These results indicate that the main factor, which defines Auger recombination rates in strongly confined NCs, is the size of the particle, while the details of the electronic structure, such as the width of the energy gap or the positions of the band minima in the $\boldsymbol{k}$-space play a minor role.

Since the topic of multiexciton dynamics in NCs of direct-gap materials such as CdSe, PbSe, and InAs, has been discussed in the literature[2,7,16,17], below we focus primarily on details of experimental studies of Ge NCs. In our work we investigate Ge NCs with radii, R, from 1.9 to 5 nm fabricated via a plasma-based technique[18,19] (see Methods for details). To monitor carrier recombination dynamics in NCs, we employ a transient absorption (TA) pump-probe spectroscopy, in which the absorption changes associated with non-equilibrium carriers injected by a sub-100 fs, 1.55 eV pump pulse are probed with a second variably delayed pulse. In the case of direct-gap NCs, the probe wavelength is normally tuned to the lowest-energy 1S absorption

feature to monitor carrier-induced band-edge bleaching[20]. Because of the small oscillator strength of inter-band (valence-to-conduction band) transitions, indirect-gap NCs do not exhibit band-edge bleaching but rather show a structureless photoinduced absorption (PA) due to intra-band transitions. Since the strength of these transitions increases with decreasing energy, PA signals are typically probed in the infra-red[21]. In our studies of Ge NCs, we used a probe wavelength of 1100 nm, which was chosen based upon signal-to-noise considerations.

In Fig. 2a we display absorption spectra of Ge NCs of two sizes in comparison to that of bulk Ge. While NC spectra do not show any distinct band-edge features typical of NCs of direct-gap semiconductors, the spectral onset of absorption shows a pronounced blue shift with respect to bulk Ge, indicating a significant role of quantum confinement. Similar trends were observed in previous linear-absorption studies of Ge NCs[22,23].

In Fig. 2b, we display TA dynamics recorded for a series of pump photon fluences from ~10^{14} cm^{-2} to 5×10^{16} cm^{-2} that correspond to NC average initial occupancy, $\langle N_0 \rangle$, from ~0.02 to 8 (estimated assuming the R^3 scaling of absorption cross sections[20], σ; see Methods). The low-intensity TA traces ($\langle N_0 \rangle \leq 0.3$) are nearly flat indicating that no significant carrier losses occur on the time scale of these measurements ($t \leq 20$ ps). As $\langle N_0 \rangle$ approaches unity and then exceeds it, a fast relaxation component of a progressively larger amplitude develops in the TA signal. This behavior is typical of Auger recombination in the regime when multiple excitons are excited per NC[2].

A more conclusive assignment of the fast TA component can be done based on the analysis of pump-intensity dependences of TA signals. At short times after excitation (t = 1 to 2 ps), the PA amplitude increases almost linearly with pump fluence across a wide range of $\langle N_0 \rangle$

from 0.01 to ~10 (inset, Fig. 2b). A similar, nearly linear scaling is observed for all NC sizes studied here (Fig. 2c), indicating that the PA amplitude provides an accurate quantitative measure of the average NC occupancy in both the single- and multiexciton regimes.

Following Auger recombination, all initially excited NCs contain only single excitons independent of their initial occupancy. Therefore, the TA signal measured immediately following Auger decay represents a measure of the total number of photoexcited NCs. When multiexitons are generated via sequential absorption of multiple photons from the same laser pulse, the distribution of initial carrier populations in a NC ensemble is described by Poisson statistics[20]. In this case, the fraction of photoexcited NCs is represented by $[1 - \exp(\langle N_0 \rangle)]$. The latter expression indeed accurately describes the TA signals measured at long times after excitation (Fig. 2d and inset of Fig. 2b). Further, using this expression as a fitting function we derive experimental absorption cross-sections, and then, compare them with calculations based on the R^3 scaling (see Methods). Good agreement between the computed and the measured values of σ (inset of Fig. 2d) together with results of pump-intensity studies of TA signals (Figs. 2c and d) support our assignment of the fast-decaying TA component to multiexciton recombination.

We derive biexciton lifetimes (τ_2) from the measured TA traces using a procedure that is explained in Methods. These lifetimes do not depend upon exact pump fluence (compare different types of symbols of the same colour in Fig. 3a), but do exhibit a pronounced size dependence. Specifically, τ_2 varies from ~4 to ~100 ps for NCs with radii from 1.9 to 5 nm, approximately following the R^3 dependence (solid line in Fig. 3b). This type of size dependence has previously been observed for Auger decay in NCs of different compositions[2,21], which

provides further evidence that the fast initial PA decay observed at high pump intensities is due to Auger recombination of multiexcitons. Furthermore, control measurements of stirred and unstirred samples (shown by different types of symbols in Fig. 3b) produce essentially identical results, indicating that processes such as NC ionization and sample photodegradation do not affect our measurements.

The efficiency of Auger recombination in bulk semiconductors is characterized by the Auger constant, C_A. Its definition suggests that Auger decay is a three-carrier process, and hence, the decay rate, r_A, is cubic in carrier density. Strictly speaking, the Auger constant cannot always be introduced for NCs because the scaling of r_A with the number of electron-hole pairs per NC, N, can vary from, for example, quadratic ($r_A \propto N^2$) to 'statistical' [$r_A \propto N^2 (N - 1)$], depending on parameters such as a material's electronic structure, NC size, and shape[4]. While recognizing this issue, we still would like to formally introduce the effective Auger constant for NCs, which provides a convenient tool for quantitative comparisons of Auger recombination efficiencies in NCs of different compositions and also between NCs and respective bulk solids.

Assuming cubic scaling of r_A with N and defining an effective carrier density as N/V_0 (V_0 is the NC volume), we obtain the following expression relating C_A to τ_2 (Ref. 4): $C_A=V_0^2(8\tau_2)^{-1}$. The C_A constants calculated for Ge NCs from the measured biexciton lifetimes are displayed in Fig. 3c in comparison to the bulk Ge value. These data show that C_A in Ge NCs (varies from 2.1×10^{-29} to 2.8×10^{-28} cm^6s^{-1}) is 3 to 4 orders of magnitude higher than the bulk Auger constant indicating a significant enhancement in the NC Auger recombination efficiency.

To explain this enhancement, we invoke relaxation of translational-momentum conservation, which occurs as a result of confinement-induced mixing between electronic states

from direct- and indirect-band minima[14,24-26]. In bulk Ge, the rate of Auger decay is greatly reduced compared to that in direct-gap semiconductors because of participation of a phonon, which compensates for a large difference in the *k*-vectors of conduction- and valence-band carriers involved in the recombination process[27] (electrons and holes are separated between the direct- and indirect-gap minima of the respective bands; Fig. 1b). Relaxation of momentum conservation in 3D confined NCs eliminates the phonon-assisted step in the Auger recombination, which makes it a lower-order, and hence, a higher probability process. This can explain the observed enhancement in Auger recombination in Ge NCs compared to bulk crystals. Previously, similar arguments have been used to explain high emission efficiencies in nanoscale forms of Si[24-26,28]. In bulk Si crystals, radiative recombination is a low-probability, phonon-assisted process. However, mixing between direct- and indirect-gap states in quantum-confined Si nanostructures leads to an increased strength of zero-phonon, pseudo-direct transitions, which greatly increases emission rates.

In addition to eliminating the need for momentum-conserving phonons in the case of indirect-gap semiconductors, relaxation in momentum conservation in NCs is expected to remove the thermal activation threshold (E_A) in Auger recombination in the case of direct-gap materials[29]. This effect must dramatically change the dependence of Auger rates on the material's energy gap since E_A is directly proportional to E_g. To determine whether Auger recombination in NCs exhibits a thermally activated behavior, we analyze the dependence of C_A on E_g.

From TA measurements conducted on PbSe and InAs NCs (not shown), we derive biexciton lifetimes, and then, use them to calculate effective Auger constants. These data are displayed in Fig. 3d together with the C_A constants derived from literature data for CdSe NCs[2].

In the same plot, we also show values of C_A for bulk PbSe[30] and InAs[12]. We further use these values to calculate C_A for NCs of different energy gaps using the bulk-like exponential dependence on E_g predicted by thermal-activation models[31,32]. The calculated values (shown by lines in Fig. 3d) exhibit much steeper drops with increasing E_g than those derived from experiment (open squares and triangles). As a result, for each given energy gap, the experimental C_A constant in NCs is orders of magnitude greater than the bulk-based projections. These observations are consistent with the expected elimination of the thermal activation threshold.

While the energy gap is a key parameter of Auger recombination in bulk direct-gap semiconductors, it should be of lesser importance in the case of "thresholdless" Auger recombination in NCs. Indeed, as evident from Fig. 3d, wide-gap CdSe and narrow-gap PbSe NCs exhibit similar values of C_A, while Auger recombination rates in bulk forms of these materials are dramatically different. Specifically, whereas Auger decay is fairly efficient in narrow-gap PbSe bulk crystals, it has never been observed in wide-gap CdSe, where radiative processes dominate (therefore, in Fig. 3d we do not show C_A for bulk CdSe). These findings are consistent with recent results of pressure-dependent studies of PbSe NCs in Ref 33, where hydrostatic pressure was used to tune the NC energy gap without significantly affecting NC size. TA studies of such "pressure-tuned" samples indicated that Auger dynamics of biexcitons remained almost unchanged despite a significant change (by more than 400 meV) in the energy gap, strongly suggesting that Auger recombination in NCs is "thresholdless", and hence, not significantly affected by E_g.

Given the above arguments, an apparent change in NC Auger rates in Fig. 3b and Auger constants in Figs. 3c and 3d is *not* due to variations in E_g but rather due to changes in NC size.

Therefore, one might expect the emergence of NC-specific trends in Auger recombination if C_A constants are analyzed as a function of NC radius instead of energy gap. Such an analysis is presented in Fig. 4 where we plot C_A versus R for NCs of Ge, PbSe, InAs, and CdSe. Remarkably, despite a vast difference in electronic structures of the bulk solids (especially when one compares direct- and indirect-gap materials), the Auger constants in same-size NCs of different compositions are similar. Further, they show a universal cubic size dependence described approximately by $C_A = \gamma R^3$. The numerical pre-factor in this expression (γ) varies by less than an order of magnitude (from 0.4×10^{-9} cm^3s^{-1} for CdSe NCs to 2.3×10^{-9} cm^3s^{-1} for Ge NCs) depending on composition, which is in sharp contrast to several orders of magnitude spread in Auger constants in corresponding bulk materials (marked on the right axis of the graph in Fig. 4).

Based on the definition of the effective Auger constant, the R^3 dependence of C_A suggests that the multiexciton decay rates (τ_N^{-1}) increase as R^{-3} with decreasing R, which is consistent with experimental results for Ge NCs in Fig. 3b as well as previous measurements of CdSe[2], InAs[16], and PbSe[7] NCs. The R^{-3} dependence indicates strong confinement-induced enhancement in Auger rates, pointing to multiple possible reasons. One is the size-dependence of the strength of confinement-induced state mixing, which facilitates Auger recombination in NCs; this effect directly depends on the ratio of R^{-1} and Δk (separation of states in k-space), and hence, is enhanced with decreasing NC size[24-26]. Further, carrier-carrier Coulomb coupling, responsible for Auger decay, is expected to scale as R^2, which also contributes to enhanced Auger decay in smaller NCs. Finally, several existing models emphasize the importance of surface effects in

Auger recombination in NCs[34,35], which may also result in increased rates of Auger decay with decreasing R because of increasing surface-to-volume ratio.

Given a large number of factors (some listed above) that can potentially affect Auger rates in NCs, it is not clear whether existing theories can explain the emergence of universal trends in the Auger process, because most of the reported theoretical studies heavily rely on specific electronic structures of individual semiconductors. However, based on our experimental findings the details of NC electronic structures are apparently of secondary importance in the Auger process, while the dominant role is played by size effects. Understanding these behaviors represents an important current challenge in the theory of multiexciton interactions in strongly confined semiconductors. This subject is also directly linked to another problem of great current interest – carrier multiplication[7,8]. The latter represents the inverse of the Auger process, and hence, new insights gained from Auger-recombination studies can greatly help in understanding the physics underlying carrier multiplication.

To summarize, a close correspondence in Auger constants and multiexciton decay rates observed for similarly sized NCs of different compositions indicates that the key parameter that defines Auger rates in these materials is NC size rather than the energy gap or electronic structure details. These observations can be rationalized by confinement-induced relaxation of momentum conservation, which removes the activation barrier in Auger decay in NCs of direct-gap semiconductors and eliminates the need for a momentum-conserving phonon in indirect-gap NCs. Thus, this effect may smear out the difference between materials with different energy gaps (E_g would normally determine the height of the activation barrier) or different arrangements of energy bands in momentum space. While the above considerations provide qualitative

understanding of experimental results, quantitative modeling of the observed universal trends requires new generalized theories of multiexciton processes in NCs capable of treating materials with very different electronic properties (direct- and indirect-gap semiconductors) in a unified framework and providing a realistic description of NC surfaces to allow for assessment of a potential impact of interfacial effects.

Methods

Ge NC synthesis. Germanium tetrachloride precursor in an argon buffer is introduced into a non-thermal, flow-through plasma reactor, as described in detail elsewhere[18,19]. $GeCl_4$ is dissociated when passing through the plasma and Ge NCs form with sizes proportional to their residence time in the plasma region. H_2 is used to scavenge Cl after dissociation. A typical NC size dispersion is in the 15-20% range. In order to passivate the Ge NC surface, a hydrogermylation reaction is performed, resulting in 1-dodecene-capped particles that can be dispersed in organic solvents (toluene was used in our optical measurements).

Absorption cross-sections. To determine the average occupancy of NCs immediately following photoexcitation ($\langle N_0 \rangle$), we use the expression $\langle N_0 \rangle = \sigma j$, where σ is the NC absorption cross-section at the pump wavelength and j is the per-pulse pump fluence measured in photons per cm^2. To estimate σ we apply the expression $\sigma = \frac{n_{Ge}}{n_{solvent}} |f|^2 V_{QD} \alpha_0$ discussed in ref. 20, where α_0 and n_{Ge} are the bulk absorption coefficient and refractive index, respectively (for bulk Ge, these values can be found in Ref. 36), $n_{solvent}$ is the matrix/solvent refractive index and f is the dielectric-confinement factor[20].

Multiexciton lifetimes. To extract the multiexciton decay component from the TA data, we subtract the slowly-varying single-exciton dynamics recorded at low intensities ($\langle N_0 \rangle << 1$) from time transients obtained at moderate pump fluences ($\langle N_0 \rangle$ from ~1 to ~10). We then derive biexciton lifetimes, τ_2, either by directly fitting decays obtained for $\langle N_0 \rangle$ close to 1 or by analyzing the higher-intensity dynamics in the region where the average exciton multiplicity, $\langle N_x \rangle$ (the average number of excitons per photoexcited NC), falls below 2. $\langle N_x \rangle$ can be determined from the ratio of the TA signal at arbitrary time to the amplitude of the slow single-excitonic background observed following fast multiexciton decay[20].

Acknowledgements This work was supported by the Chemical Sciences, Biosciences and Geosciences Division of the Office of Basic Energy Sciences, U.S. Department of Energy (DOE) and Los Alamos LDRD funds. V.I.K. acknowledges partial support from the Center for Integrated Nanotechnologies jointly operated for DOE by Los Alamos and Sandia National Laboratories. R.G. and U.K. acknowledge partial support by the MRSEC Program of the National Science Foundation under Award Number DMR-0212302 and DMR-0819885 and by the University of Minnesota Center for Nanostructure Applications.

Competing interests statement The authors declare that they have no competing financial interests.

Correspondence and requests for materials should be addressed to V.I.K. (klimov@lanl.gov).

References

1. Chepic, D.I. et al. Auger ionization of semiconductor quantum drops in a glass matrix. *Journal of Luminescence* **47**, 113-127 (1990).
2. Klimov, V.I., Mikhailovsky, A.A., McBranch, D.W., Leatherdale, C.A. & Bawendi, M.G. Quantization of Multiparticle Auger Rates in Semiconductor Quantum Dots. *Science* **287**, 1011-1013 (2000).
3. Wang, L.-W., Califano, M., Zunger, A. & Franceschetti, A. Pseudopotential Theory of Auger Processes in CdSe Quantum Dots. *Physical Review Letters* **91**, 056404 (2003).
4. Klimov, V.I., McGuire, J.A., Schaller, R.D. & Rupasov, V.I. Scaling of multiexciton lifetimes in semiconductor nanocrystals. *Physical Review B (Condensed Matter and Materials Physics)* **77**, 195324 (2008).
5. Klimov, V.I. et al. Optical Gain and Stimulated Emission in Nanocrystal Quantum Dots. *Science* **290**, 314-317 (2000).
6. Klimov, V.I. et al. Single-exciton optical gain in semiconductor nanocrystals. *Nature* **447**, 441-446 (2007).
7. Schaller, R.D. & Klimov, V.I. High Efficiency Carrier Multiplication in PbSe Nanocrystals: Implications for Solar Energy Conversion. *Physical Review Letters* **92**, 186601-4 (2004).
8. Ellingson, R.J. et al. Highly Efficient Multiple Exciton Generation in Colloidal PbSe and PbS Quantum Dots. *Nano Lett.* **5**, 865-871 (2005).
9. Nozik, A.J. Quantum dot solar cells. *Physica E: Low-dimensional Systems and Nanostructures* **14**, 115-120 (2002).
10. Landsberg, P.T. *Recombination in Semiconductors*, (Cambridge University Press).
11. Haug, A. Band-to-band Auger recombination in semiconductors. *Journal of Physics and Chemistry of Solids* **49**, 599-605 (1988).
12. Vodopyanov, K.L., Graener, H., Phillips, C.C. & Tate, T.J. Picosecond carrier dynamics and studies of Auger recombination processes in indium arsenide at room temperature. *Physical Review B* **46**, 13194 (1992).
13. Auston, D.H., Shank, C.V. & LeFur, P. Picosecond Optical Measurements of Band-to-Band Auger Recombination of High-Density Plasmas in Germanium. *Physical Review Letters* **35**, 1022 (1975).
14. Cullis, A.G., Canham, L.T. & Calcott, P.D.J. The structural and luminescence properties of porous silicon. *Journal of Applied Physics* **82**, 909-965 (1997).
15. Fauchet, P.M. Photoluminescence and electroluminescence from porous silicon. *Journal of Luminescence* **70**, 294-309 (1996).
16. Schaller, R.D., Pietryga, J.M. & Klimov, V.I. Carrier Multiplication in InAs Nanocrystal Quantum Dots with an Onset Defined by the Energy Conservation Limit. *Nano Lett.* **7**, 3469-3476 (2007).
17. Wehrenberg, B.L., Wang, C. & Guyot-Sionnest, P. Interband and Intraband Optical Studies of PbSe Colloidal Quantum Dots. *J. Phys. Chem. B* **106**, 10634-10640 (2002).
18. Gresback, R., Holman, Z. & Kortshagen, U. Nonthermal plasma synthesis of size-controlled, monodisperse, freestanding germanium nanocrystals. *Applied Physics Letters* **91**, 093119 (2007).
19. Cernetti, P., Gresback, R., Campbell, S.A. & Kortshagen, U. Nonthermal Plasma Synthesis of Faceted Germanium Nanocrystals. *Chemical Vapor Deposition* **13**, 345-350 (2007).
20. Klimov, V.I. Optical Nonlinearities and Ultrafast Carrier Dynamics in Semiconductor Nanocrystals. *J. Phys. Chem. B* **104**, 6112-6123 (2000).
21. Beard, M.C. et al. Multiple Exciton Generation in Colloidal Silicon Nanocrystals. *Nano Lett.* **7**, 2506-2512 (2007).

22. James, R.H., Shiang, J.J. & Alivisatos, A.P. Germanium quantum dots: Optical properties and synthesis. *The Journal of Chemical Physics* **101**, 1607-1615 (1994).
23. Wilcoxon, J.P., Provencio, P.P. & Samara, G.A. Synthesis and optical properties of colloidal germanium nanocrystals. *Physical Review B* **64**, 035417 (2001).
24. Hybertsen, M.S. Absorption and emission of light in nanoscale silicon structures. *Physical Review Letters* **72**, 1514 (1994).
25. Kovalev, D. et al. Breakdown of the k-Conservation Rule in Si Nanocrystals. *Physical Review Letters* **81**, 2803 (1998).
26. Sykora, M. et al. Size-Dependent Intrinsic Radiative Decay Rates of Silicon Nanocrystals at Large Confinement Energies. *Physical Review Letters* **100**, 067401 (2008).
27. Huldt, L. Phonon-assisted Auger recombination in germanium. *Physica Status Solidi (a)* **33**, 607-614 (1976).
28. Canham, L.T. Silicon quantum wire array fabrication by electrochemical and chemical dissolution of wafers. *Applied Physics Letters* **57**, 1046-1048 (1990).
29. Kharchenko, V.A. & Rosen, M. Auger relaxation processes in semiconductor nanocrystals and quantum wells. *Journal of Luminescence* **70**, 158-169 (1996).
30. Klann, R., Hofer, T., Buhleier, R., Elsaesser, T. & Tomm, J.W. Fast recombination processes in lead chalcogenide semiconductors studied via transient optical nonlinearities. *Journal of Applied Physics* **77**, 277-286 (1995).
31. Emtage, P.R. Auger recombination and junction resistance in lead-tin telluride. *Journal of Applied Physics* **47**, 2565-2568 (1976).
32. Beattie, A.R. & Landsberg, P.T. Auger Effect in Semiconductors. *Proceedings of the Royal Society of London. Series A, Mathematical and Physical Sciences* **249**, 16-29 (1959).
33. Pietryga, J.M., Zhuravlev, K.K., Klimov, V.I. & Schaller, R.D. Evidence for barrier-less Auger recombination in PbSe nanocrystals: A pressure-dependent study of transient optical absorption. *Physical Review Letters, in press* (2008).
34. Efros, A.L., Lockwood, D.J. & Tsybeskov, L. (eds.). *Semiconductor Nanocrystals: From Basic Principles to Applications*, (Kluwer, New York, 2003).
35. Pandey, A. & Guyot-Sionnest, P. Multicarrier recombination in colloidal quantum dots. *The Journal of Chemical Physics* **127**, 111104 (2007).
36. Adachi, S. Optical dispersion relations for Si and Ge. *Journal of Applied Physics* **66**, 3224-3231 (1989).

Figure captions

Figure 1. Auger recombination in direct- and indirect-gap semiconductors. a, Three-particle Auger process in direct-gap bulk semiconductors. **b,** Phonon-assisted four-particle Auger process in indirect-gap bulk semiconductors; numbers indicate the sequence of events. **c,** Auger recombination in NCs. Strong spatial confinement in NCs leads to relaxation of momentum conservation requirements, which diminishes the difference between direct- and indirect-gap materials with regard to the Auger process.

Figure 2. Linear- and transient-absorption properties of Ge NCs. a, Linear absorption spectra of Ge NCs indicate an absorption onset, which is blue-shifted compared to bulk Ge. Insets: Examples of large-area (upper left corner) and high-resolution (lower right corner) transmission electron micrographs of Ge NCs indicating size-monodispersity and a high degree of crystallinity. **b,** Pump-intensity-dependent TA dynamics of 1.85 nm radius Ge NCs for average initial occupancies from 0.02 to 8.3. The fast initial decay component is due to multiexciton recombination. Inset: Pump-intensity dependence of early- and late-time TA signals for Ge NCs with R = 1.85 nm. Saturation of the long-time signal observed for large $\langle N_0 \rangle$ occurs because following Auger recombination, all photoexcited NCs contain single excitons independent of their initial occupancies **c,** Pump-intensity dependence of TA signals shortly after excitation for Ge NCs with radii of 1.85, 2.75, and 5.0 nm (symbols) fit to a linear dependence (line). **d,** Long-time TA signals ($t >> \tau_2$) as a function of $\langle N_0 \rangle$ fit to the Poissonian dependence describing the total number of photoexcited NCs. Inset: Absorption cross-sections (symbols) derived from fits to experimental data in the main panel in comparison to calculations based on

the R^3 scaling (line; the shaded region shows the range of uncertainty due to the distribution in NC sizes).

Figure 3. Multiexciton dynamics and Auger constants in semiconductor NCs. a, Biexcitonic decay component in Ge NCs as a function of NC size. Symbols are colour-coded according to NC size, while different styles correspond to different initial occupancies. **b,** Biexciton lifetimes in Ge NCs measured for stirred and unstirred solution samples (squares and circles, respectively) as a function of NC radius fit to the R^3 dependence (line). **c,** Auger constants of bulk (solid square) and nanocrystalline (open square) Ge as a function of energy gap. **d,** Comparison of C_A in bulk (solid symbols) and nanocrystalline (open symbols) forms of direct gap semiconductors PbSe (squares), InAs (triangles) and CdSe (circles) as a function of energy gap. Lines are projected values of C_A based on bulk-like exponential dependences of Auger constants on E_g.

Figure 4. Universal size-dependence of Auger constants in semiconductor NCs. When plotted as a function of NC radius, C_A values for NCs of both direct- and indirect-gap semiconductors show a similar size dependence described by $C_A = \gamma R^3$.

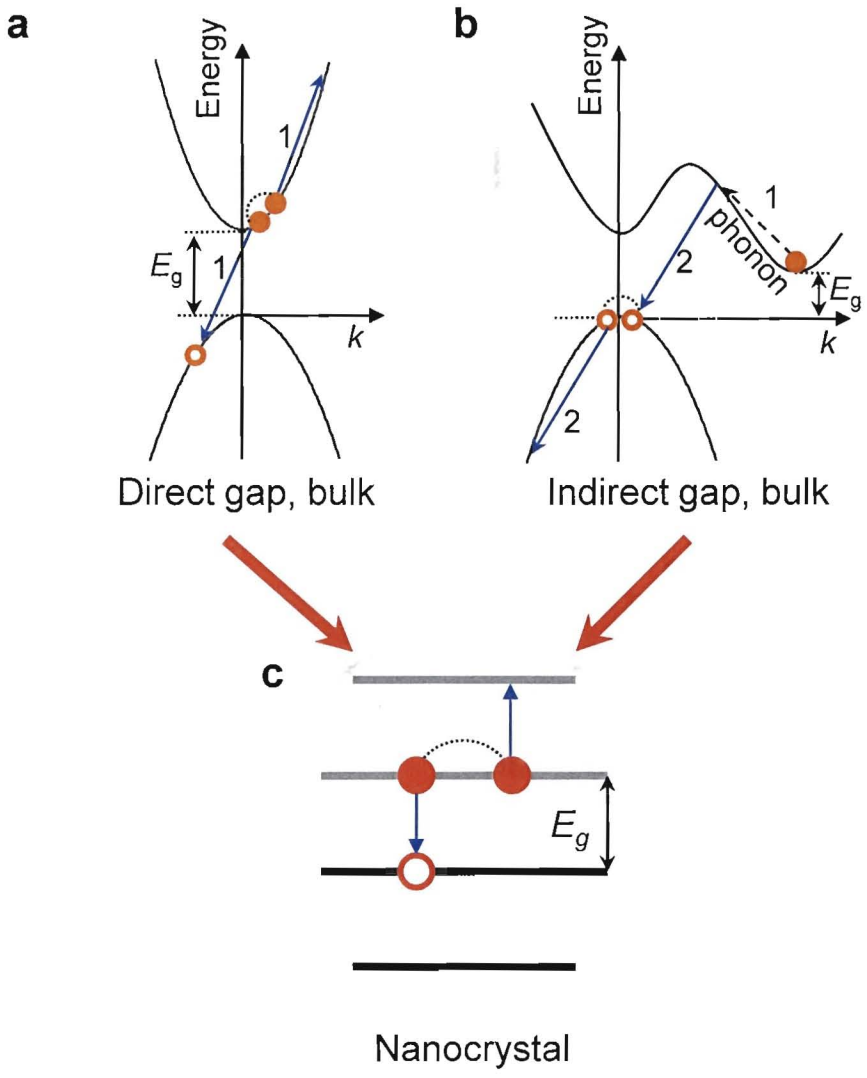
a
Energy
1
E_g
1
k
Direct gap, bulk
b
Energy
1
phonon
2
E_g
k
2
Indirect gap, bulk
c
E_g
Nanocrystal

Figure 1.

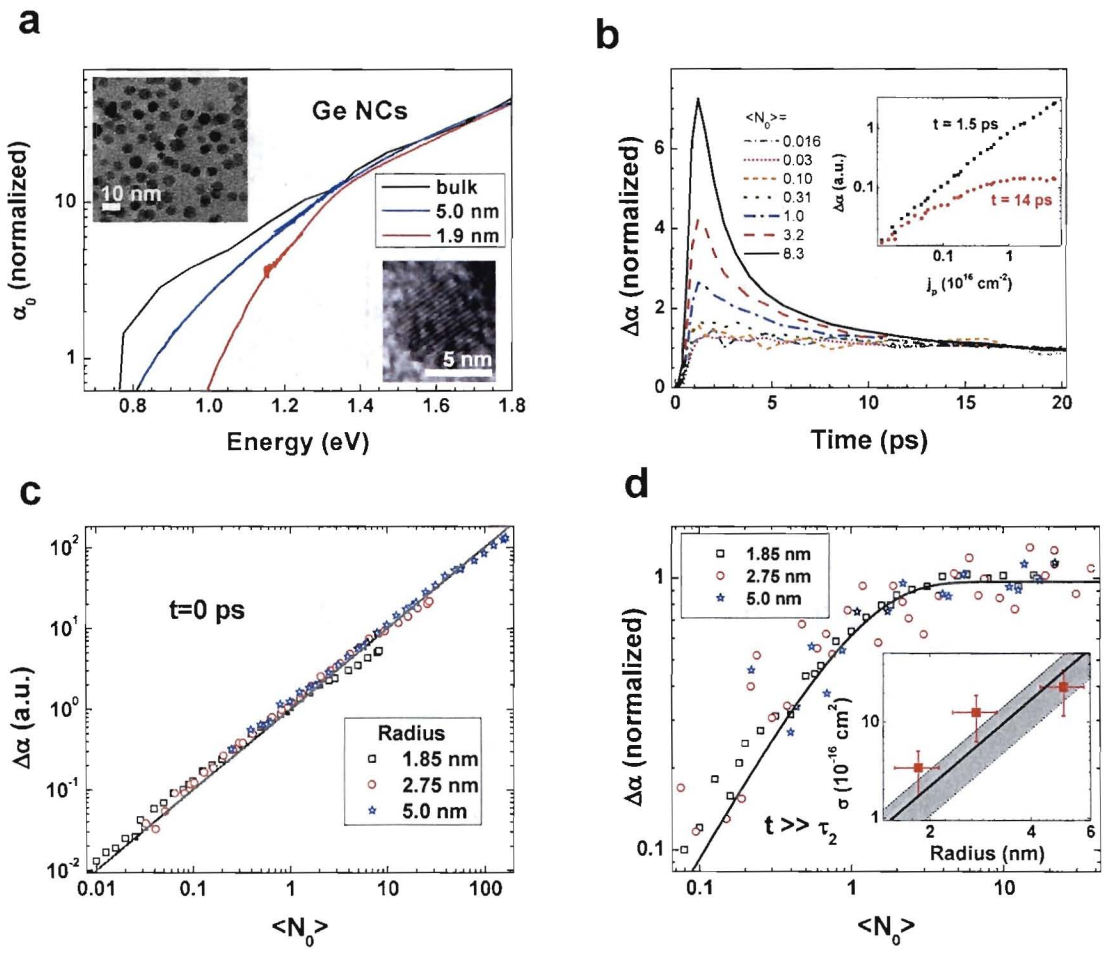
a
Ge NCs
10 nm
5 nm
bulk
5.0 nm
1.9 nm
α0 (normalized)
Energy (eV)
b
<N0>=
0.016
0.03
0.10
0.31
1.0
3.2
8.3
t = 1.5 ps
t = 14 ps
Δα (a.u.)
jp (10^16 cm^-2)
Δα (normalized)
Time (ps)
c
t=0 ps
Radius
1.85 nm
2.75 nm
5.0 nm
Δα (a.u.)
<N0>
d
1.85 nm
2.75 nm
5.0 nm
t >> τ2
σ (10^-16 cm^2)
Radius (nm)
Δα (normalized)
<N0>

Figure 2.

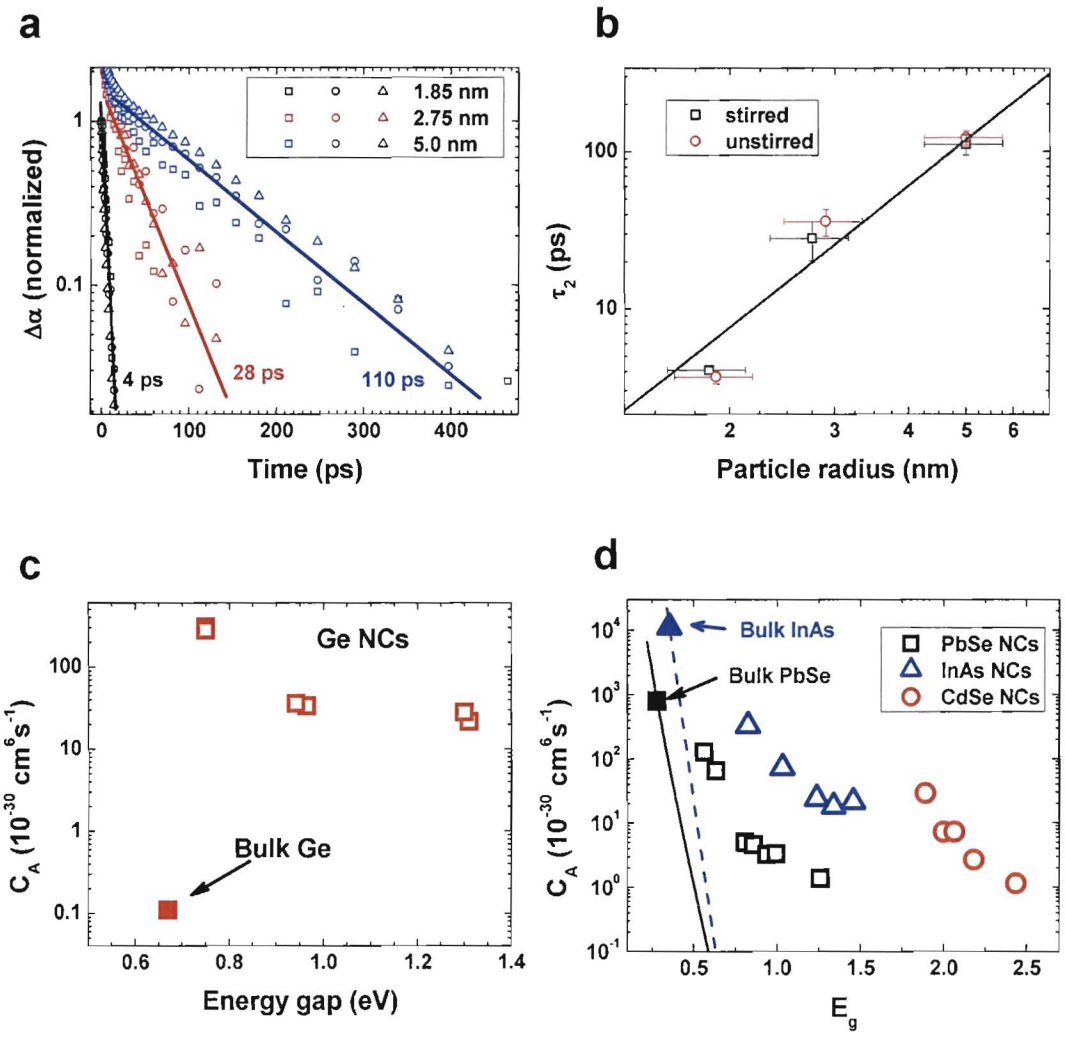
a
Δα (normalized)
1
0.1
1.85 nm
2.75 nm
5.0 nm
4 ps
28 ps
110 ps
0
100
200
300
400
Time (ps)
b
τ2 (ps)
100
10
stirred
unstirred
2
3
4
5
6
Particle radius (nm)
c
CA (10-30 cm6s-1)
100
10
1
0.1
Ge NCs
Bulk Ge
0.6
0.8
1.0
1.2
1.4
Energy gap (eV)
d
CA (10-30 cm6s-1)
10^4
10^3
10^2
10^1
10^0
10^-1
Bulk InAs
Bulk PbSe
PbSe NCs
InAs NCs
CdSe NCs
0.5
1.0
1.5
2.0
2.5
Eg

Figure 3.

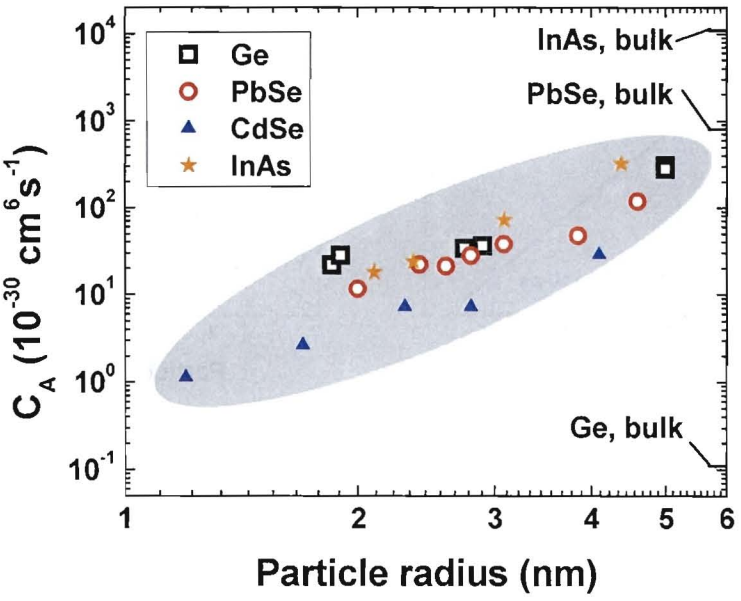
Ge
PbSe
CdSe
InAs
InAs, bulk
PbSe, bulk
Ge, bulk
C_A (10^{-30} cm^6 s^{-1})
Particle radius (nm)
10^4
10^3
10^2
10^1
10^0
10^{-1}
1
2
3
4
5
6

Figure 4.